PERGAMON

International Journal of Solids and Structures 40 (2003) 4925–4940

INTERNATIONAL JOURNAL OF SOLIDS and STRUCTURES

www.elsevier.com/locate/ijsolstr

Transient dynamic responses of a cracked solid subjected to in-plane loadings

S.W. Liu [a], Jin H. Huang [b,*]

[a] *Department of Electrical Engineering, Chin Min College, 110 Shyue Fu Road, Tou-Fen, Taiwan 351 People's Republic of China*
[b] *Department of Mechanical and Computer Aided Engineering, Feng Chia University, 100 Wen Hwa Road Seatwen, Taichung, Taiwan 40745, People's Republic of China*

Received 29 June 2001; received in revised form 31 March 2003

Abstract

Transient dynamic responses of an elastic cracked solid subjected to in-plane surface loadings are investigated in this study. Two vertical cracks, a surface-breaking crack and a sub-surface crack, are considered. The frequency responses of the plane strain problem are calculated by the computational mechanics combining the finite element method with the boundary integral equation. The finite element method is used for the near-field enclosing the crack, while the boundary integral equation is applied for the far-field to satisfy the Sommerfeld radiation condition. The transient responses are then obtained using fast Fourier transform. Surface displacements, crack opening displacements, and dynamic stress intensity factors are presented to show the significant effects of the cracks. The interaction between the elastic waves and the cracks as well as the mode conversion phenomena can be observed and understood through the numerical simulations.

Keywords: Scattering; Ultrasonic nondestructive testing; Crack opening displacements; Dynamic stress intensity factors; Mode conversion

1. Introduction

Cracks can cause significant changes in the mechanical behavior of materials and the integrity of structures, the most dramatic change being the possibility of fracture. The ultrasonic techniques in which elastic waves propagate through the material and are scattered by the crack are often utilized for the nondestructive detection of cracks. From the features of the scattering, the detection and characterization of the crack can be attempted. Recently, a review of ultrasonic quantitative nondestructive evaluation (NDE) focused on the detection of cracks can be found in Achenbach (2000). On the other hand, in the context of elastodynamic fracture mechanics, the main emphasis is placed on determining the stress intensity factor as a function of time and of geometrical and material parameters. An important class of problems concerns the diffraction of

* Corresponding author. Fax: +886-4-245-6545/4516545.
E-mail address: jhhuang@fcu.edu.tw (J.H. Huang).

0020-7683/03/$ - see front matter © 2003 Elsevier Ltd. All rights reserved.
doi:10.1016/S0020-7683(03)00276-2

the elastic waves by a pre-existing crack in the material. For a crack existing in the particular load-carrying member, it is necessary to evaluate the stress intensity factor for a critical size of the crack in order to check whether the fracture toughness of the material is exceeded or not. In particular for stress wave loading, dynamic overshoots of stress intensity factors are possible. Therefore, it is of importance to understand the physical phenomenon of the elastic wave scattering by cracks beforehand.

In two-dimensional elastodynamics, two mutually uncoupled kinds of wave motion exist, viz., horizontally polarized shear wave motion (SH waves or anti-plane motion) and vertically polarized wave motion (P and SV waves or in-plane motion). The case of anti-plane motion is particularly attractive because of the simple nature of the interaction of SH waves with cracks and other boundaries. Therefore, the problems of anti-plane motion have been studied extensively by a number of authors. The diffraction of SH waves by an edge crack was investigated by Datta (1979) using a matched asymptotic expansion as well as a combined finite element and analytical expansion technique. Ma and Chen (1994) solved analytically the transient response of a half-space containing an inclined sub-surface semi-infinite crack by using the superposition of the fundamental solutions in the Laplace transform domain. The scattering of time harmonic waves by a rough crack were studied by Boström et al. (1994) using an extension of the null field approach. The responses of a cracked half-space subjected to an incident SH plane wave and an anti-plane impact loading have been investigated in detail by Liu et al. (1997) and Liu et al. (1998), respectively. The depth of the crack-tip can be estimated from the diffracted waves received at the free surface. The resonance frequencies are closely related to the crack length. Zhang (2000) presented the dynamic stress intensity factors of an anti-plane crack in anisotropic solids using a boundary integral equation method.

For the case of in-plane motion, the scattering of elastic waves is more complicated due to the phenomena of mode conversion. Few analytical solutions are available. More general and realistic problems must be treated by numerical method, for instance, finite difference methods, finite element methods, boundary element methods, T-matrix methods, etc. The excitation of Rayleigh waves at surface discontinuities (steps and slots) due to body waves incidence were investigated by Saffari and Bond (1987) using explicit finite difference method. The numerical modelling work showed that mode-converted Rayleigh waves are a strong feature of the scattering at surface-breaking slots. These results were also backed up by experimental observations. Scandrett and Achenbach (1987) calculated the interaction of an ultrasonic wave with a surface-breaking crack by the use of the finite difference method. A modified finite-difference grid was derived by Saenger et al. (2000) to solve the problems of high contrasts of the medium parameters, which could cause instability problems for a standard staggered grid. Although the finite difference method is a powerful tool for the problem of wave propagation, it has difficulty to treat the problem of very narrow cracks. The finite element method is superior to the other methods because of its versatility to model flaws of arbitrary shape and size, and its ability to incorporate anisotropic and inhomogeneous material nature with ease. The finite element method combined with particle models were used by Harumi and Uchida (1990) for the computer simulation of ultrasound and its applications. A plane strain finite element model with absorbing boundary condition was used by Datta and Kishore (1996) and Kishore et al. (2000) to simulate the scattering of ultrasonic waves in isotropic and orthotropic solids with or without the presence of flaws. A hybrid method combining T-matrix and boundary element was used by Wang and Shen (1997) to study the scattering of elastic waves by a crack in a plate.

Dynamic stress intensity factors for buried planar and nonplanar cracks in a half-space were studied by Shah et al. (1986) using a hybrid numerical technique combining a multipolar representation of the scattered field with the finite element method. The closed form solutions of the stress intensity factor of a subsurface inclined semi-infinite crack in a half-space were given by Tsai and Ma (1993) using linear superposition of the fundamental solution in the Lapalace transform domain. Based on integral transforms and an asymptotic usage of the Wiener–Hopf technique, exact expressions for the elastodynamic stress intensity factor at the tip of a long external crack in a strip-like body were analyzed by Georgiadis and Brock (1994).

Because each method has its own advantages and disadvantages, a hybrid method combining the finite element method with the boundary integral equation is adopted in this study. The finite element method is applied to the near-field enclosing completely the scatterers, while the boundary integral equation is used for the far-field to satisfy the Sommerfeld radiation condition. By using this hybrid method, the full field solutions can be obtained without the problem of spurious reflections from the artificial boundaries of the computation domain.

This paper is concerned with the scattering that results from the interaction of cracks with elastic waves generated by a short pulse at the free surface of a semi-infinite solid. The results of our research may be of considerable interest to both quantitative NDE of structures and fracture mechanics. A problem of special interest to NDE and fracture mechanics is the diffraction by a near-surface crack. Therefore, two types of cracks, a surface-breaking crack and a sub-surface crack, are considered in this study. Numerical results are presented for surface displacements, crack opening displacements, and dynamic stress intensity factors to show the significant effects of the cracks. The numerical study revealed some interesting features of the problem. Strong Rayleigh waves are always produced at the free surface of the half-space. The interaction between impact stress waves and cracks may cause overshoots for dynamic stress intensity factors. Both reflected and diffracted waves are not only clearly observed at the free surface but also strongly related to the characteristics of the crack.

2. Statement of the problem

A two-dimensional cracked solid subjected to an in-plane time-dependent loading as shown in Fig. 1 is considered in the present analysis. The material response is assumed to be linear elastodynamic. The crack is considered to be a surface of displacement discontinuity, which cannot transmit surface tractions. The faces of a crack are infinitesimally close prior to ultrasonic excitation, and they do not interact when the solid has been excited. This is an acceptable approximation for real cracks if the faces do not touch when the solid is disturbed. This problem is first solved in frequency domain, then the transient responses is obtained by the fast Fourier transform. Let the displacement $\mathbf{u}(x,z,t)$ has time harmonic behavior of the form $\mathbf{u}(x,z)\mathrm{e}^{-\mathrm{i}\omega t}$, where ω is the circular frequency and t is the time. The wave equation for homogeneous isotropic elasticity theory in frequency domain, in terms of the displacement $\mathbf{u}(x,z)$, is given by

$$(\lambda+2\mu)\nabla\nabla\cdot\mathbf{u}-\mu\nabla\times\nabla\times\mathbf{u}+\mathbf{f}=-\rho\omega^2\mathbf{u}, \tag{1}$$

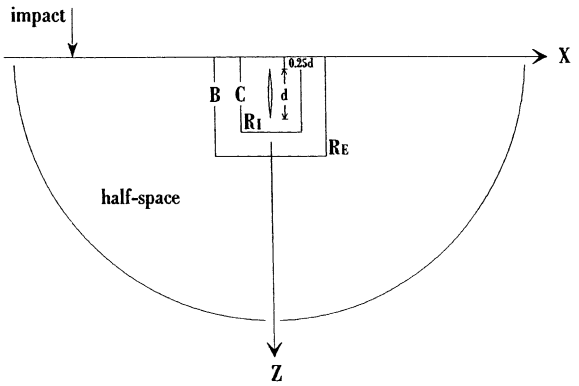

Fig. 1. Configuration of a cracked solid subjected to an in-plane loading at the free surface.

where, λ and μ are the Lamé elastic constants, ρ is the material density, $\mathbf{f}$ is the body force, and the factor $e^{-i\omega t}$ has been dropped. Boundary conditions include traction-free conditions for crack faces and the surface of the half-space and the Sommerfeld radiation conditions.

In order to solve the problem by the hybrid method considered here, an artificial boundary B and a contour C are introduced as shown in Fig. 1. The crack is completely enclosed by the contour C. The interior region R_I is the near-field bounded by the boundary B, while the exterior region R_E is the far-field bounded inside by contour C. The region between boundary B and contour C belongs to the interior as well as exterior and the overlap is for sidestepping singularities in calculations of Green's functions. It has been possible to move the observation points (on C) away from the source points (on B). Thus the singularities of the Green's functions are avoided and the desired numerical accuracy can be assured. The finite element technique is used for the interior region and the boundary integral representation along contour C for the displacements on boundary B is used to solve the scattered field in the exterior region.

3. Boundary integral equation

The boundary integral equation is derived by means of the Betti's reciprocal theorem and used in the exterior region to obtain the scattered field solutions. Here the total field displacement $\mathbf{u}$ can be specified by

$$\mathbf{u} = \mathbf{u}^{(i)} + \mathbf{u}^{(s)}, \tag{2}$$

where $\mathbf{u}^{(i)}$ is the incident field displacement and $\mathbf{u}^{(s)}$ the scattered field. For the problem considered in this study, the incident field can be obtained by solving the Green's problem that is a flawless solid subjected to a concentrated unit load. The equation of Green's problem with source located at the point (ξ, ζ) is given by

$$\Sigma_{ijk,k} + \rho\omega^2 G_{ij} = -\delta_{ij}\delta(x-\xi)\delta(z-\zeta), \tag{3}$$

where i denotes the force direction, j stands for the displacement direction, G_{ij} and Σ_{ijk} are the Green's displacements and the corresponding stresses. By applying the traction-free boundary condition and the radiation condition to the homogeneous half-space, the Green's functions in Eq. (3) can be obtained. The explicit solutions are expressed in Liu et al. (1996). The numerical results were achieved through an effective quadrature scheme given by Xu and Mal (1987). The scattered field is represented by a line integral based on the Betti's reciprocal theorem. In this reciprocity theorem, two different elastodynamic states are employed. The two-dimensional reciprocity theorem over contour C can be expressed in the following form,

$$\iint_{\mathbf{A}} (\mathbf{f}^{(I)} \cdot \mathbf{u}^{(II)} - \mathbf{f}^{(II)} \cdot \mathbf{u}^{(I)})\, dA = \oint_C (\mathbf{u}^{(I)} \cdot \mathbf{s}^{(II)} - \mathbf{u}^{(I)} \cdot \mathbf{s}^{(II)})\, dC, \tag{4}$$

where $\mathbf{u}^{(I)}$ and $\mathbf{s}^{(I)}$ are the displacement and surface traction caused by the body force $\mathbf{f}^{(I)}$, and $\mathbf{u}^{(II)}$ and $\mathbf{s}^{(II)}$ denote the displacement and surface traction due to the body force $\mathbf{f}^{(II)}$, respectively.

The Betti's reciprocal theorem is first applied to the exterior region. Two states considered here are scattered field and Green's field with source (ξ, ζ) located at boundary B. There are no defects in the exterior region so that the body force of scattered field is zero. Using the reciprocal theorem these two states can be related in the following manner,

$$u_i^{(s)}(\xi, \zeta) = \oint_C \left(u_j^{(s)} \Sigma_{ijk} - G_{ij}\sigma_{jk}^{(s)} \right) n_k\, dC, \tag{5}$$

where $u_i^{(s)}$ and $\sigma_{jk}^{(s)}$ denotes the displacement and stress tensor of scattered field, and n_k is the component of outward unit normal to contour C. Next, the reciprocal theorem is applied to the region bounded by contour C. The incident field and the Green's field are the two states considered here. There are no body forces for both fields in this region, thus Eq. (4) becomes

$$0 = \oint_C \left(u_j^{(\mathrm{i})} \Sigma_{ijk} - G_{ij} \sigma_{jk}^{(\mathrm{i})} \right) n_k \, \mathrm{d}C, \tag{6}$$

where $u_j^{(\mathrm{i})}$ and $\sigma_{jk}^{(\mathrm{i})}$ denotes the displacement and stress of the incident field.

Combining Eqs. (5) and (6), the displacement for scattered field at point (ξ, ζ) can be represented by the following integral form,

$$u_i^{(\mathrm{s})}(\xi, \zeta) = \oint_C \left(u_j \Sigma_{ijk} - G_{ij} \sigma_{jk} \right) n_k \, \mathrm{d}C. \tag{7}$$

Then the displacement for total field is given by

$$u_i(\xi, \zeta) = \oint_C \left(u_j \Sigma_{ijk} - G_{ij} \sigma_{jk} \right) n_k \, \mathrm{d}C + u_i^{(\mathrm{i})}(\xi, \zeta). \tag{8}$$

This integral representation can be used to calculate the total field at any point in the exterior region. However, the evaluation of the integration is impossible without the scattered field solution at contour C. This can be achieved with the aid of finite element method.

4. Finite element method

The finite element method deals with the solution in the interior region, which encloses all the flaws in the material. The interior region is discretized into a number of finite elements. The mesh size is chosen such that approximately ten nodes exist in a distance of one smallest wavelength for a reasonable numerical accuracy. The area between boundary B and contour C is discretized by one layer of seven-node elements with two nodes on boundary B. In order to simulate the stress concentration near the crack-tips, six-node triangular quarter-point singular elements has been used around the crack-tips. The rest are eight-node quadrilateral elements. The displacement interior to the elements can be expressed in terms of the shape functions ($\mathbf{\Phi}$) and nodal displacements ($\mathbf{d}_e$) in the matrix form as follows:

$$\mathbf{u}_e = \begin{Bmatrix} u_x \\ u_z \end{Bmatrix}_e = \begin{bmatrix} \phi_1 & 0 & \cdots & \phi_n & 0 \\ 0 & \phi_1 & \cdots & 0 & \phi_n \end{bmatrix} \begin{Bmatrix} u_{x1} \\ u_{z1} \\ \vdots \\ u_{xn} \\ u_{zn} \end{Bmatrix}_e = \Phi \mathbf{d}_e, \tag{9}$$

where subscript e is the element identifier and n is the number of nodes per element. The strain within an element can be written in terms of nodal displacements as the following:

$$\boldsymbol{\varepsilon} = \mathbf{D}\mathbf{u}_e = \mathbf{B}\mathbf{d}_e, \tag{10}$$

where $\mathbf{B} = \mathbf{D}\mathbf{\Phi}$ and $\mathbf{D}$ is an operator matrix defined as

$$\mathbf{D} = \begin{bmatrix} \dfrac{\partial}{\partial x} & 0 \\ 0 & \dfrac{\partial}{\partial z} \\ \dfrac{\partial}{\partial z} & \dfrac{\partial}{\partial x} \end{bmatrix}. \tag{11}$$

The relationship between the stress and the strain is given by

$$\boldsymbol{\sigma} = \mathbf{C}\boldsymbol{\varepsilon}, \tag{12}$$

where $\mathbf{C}$ is a 3×3 symmetric matrix of the material elastic constants in the element.

In order to determine the elemental impedance matrix, let us consider the energy function of the element,

$$E_e = \frac{1}{2}\iint_{A_e}(\boldsymbol{\sigma}^*\boldsymbol{\varepsilon} - \rho\omega^2\mathbf{u}^*\mathbf{u})\,\mathrm{d}x\,\mathrm{d}z - \frac{1}{2}\int_l(\mathbf{u}^*\mathbf{s} + \mathbf{s}^*\mathbf{u})\,\mathrm{d}l, \tag{13}$$

where * denotes the conjugate transpose. The first term in Eq. (13) includes the strain and kinetic energies, while the second term is the surface traction work potential. Substituting Eqs. (9), (10), and (12) into Eq. (13) and taking the variation with respect to $\mathbf{u}^*$, the equation of motion for each element can be written in the following form,

$$(\mathbf{K}_e - \omega^2\mathbf{M}_e)\mathbf{d}_e = \mathbf{p}_e, \tag{14}$$

where $\mathbf{K}_e$ is the stiffness matrix determined by the elastic properties of the element, $\mathbf{M}_e$ is the mass matrix determined by the density distribution of the element, and $\mathbf{p}_e$ is the nodal force vector. Then the global equation of motion can be obtained by assembling the elemental equations of motion,

$$(\mathbf{K} - \omega^2\mathbf{M})\mathbf{d} = \mathbf{p}. \tag{15}$$

Both the stiffness and mass matrices are large, sparse, symmetric and positive definite that can be stored effectively by adequate techniques. Eq. (15) can be written in terms of impedance matrix $\mathbf{S}$ as follows:

$$\mathbf{S}\mathbf{d} = \mathbf{p}. \tag{16}$$

The nodal displacement $\mathbf{d}_\mathrm{B}$ at boundary B can be separated from the interior nodal displacement $\mathbf{d}_\mathrm{I}$. Thus Eq. (16) is partitioned into the following form,

$$\begin{bmatrix}\mathbf{S}_{\mathrm{BB}} & \mathbf{S}_{\mathrm{BI}}\\ \mathbf{S}_{\mathrm{IB}} & \mathbf{S}_{\mathrm{II}}\end{bmatrix}\begin{Bmatrix}\mathbf{d}_\mathrm{B}\\ \mathbf{d}_\mathrm{I}\end{Bmatrix} = \begin{Bmatrix}\mathbf{p}_\mathrm{B}\\ \mathbf{p}_\mathrm{I}\end{Bmatrix}, \tag{17}$$

where $\mathbf{p}_\mathrm{B}$ denotes the nodal force at the boundary B and $\mathbf{p}_\mathrm{I}$ the interior nodal force. This completes the analysis of the finite element formulation for the near field.

5. Solutions

The solution of the problem can be obtained by coupling the finite element equations with the boundary integral equations. Making use of finite element formulations from Eqs. (9), (10), and (12), the evaluation of Eq. (8) for all nodes on the boundary B becomes

$$\mathbf{d}_\mathrm{B} = \mathbf{d}_\mathrm{B}^{(\mathrm{i})} + \mathbf{A}_{\mathrm{BI}}\mathbf{d}_\mathrm{I} + \mathbf{A}_{\mathrm{BB}}\mathbf{d}_\mathrm{B}, \tag{18}$$

where $\mathbf{d}_\mathrm{B}^{(\mathrm{i})}$ is the incident field displacement at the boundary B, $\mathbf{A}_{\mathrm{BI}}$ and $\mathbf{A}_{\mathrm{BB}}$ are complex matrices. Combining Eq. (18) with the second equation of Eq. (17), one gets

$$\begin{bmatrix}\mathbf{I} - \mathbf{A}_{\mathrm{BB}} & -\mathbf{A}_{\mathrm{BI}}\\ \mathbf{S}_{\mathrm{IB}} & \mathbf{S}_{\mathrm{II}}\end{bmatrix}\begin{Bmatrix}\mathbf{d}_\mathrm{B}\\ \mathbf{d}_\mathrm{I}\end{Bmatrix} = \begin{Bmatrix}\mathbf{d}_\mathrm{B}^{(\mathrm{i})}\\ \mathbf{p}_\mathrm{I}\end{Bmatrix}. \tag{19}$$

The total nodal displacements ($\mathbf{d}_\mathrm{B}$ and $\mathbf{d}_\mathrm{I}$) at a certain frequency can be obtained by solving Eq. (19). The complex matrix in Eq. (19) is usually large, sparse, and unsymmetrical. In order to reduce the required memory of computation, a compacted data structure is used to store the nonzero terms of the sparse matrix in a column list scheme. Then an iterative method, the biconjugate gradient method, is adopted instead of usual direct methods to solve Eq. (19). These techniques not only are very efficient but also provide a satisfaction solution. Once the nodal displacements in the near filed are obtained, the full field solutions any where in the domain can be easily calculated either by the finite element formulation of Eq. (9) or by the boundary integral representation of Eq. (8).

For vertical cracks considered in this study, the horizontal and vertical crack opening displacements (C_x and C_z) are given by

$$C_x = u_x(0^+, z) - u_x(0^-, z), \tag{20}$$

$$C_z = u_z(0^+, z) - u_z(0^-, z). \tag{21}$$

The stress intensity factors K_{I} and K_{II} can be computed from the crack opening displacements near a crack-tip by the following relations (Shah et al., 1986)

$$\begin{Bmatrix} K_{\mathrm{I}} \\ K_{\mathrm{II}} \end{Bmatrix} = \frac{\mu}{4(1-\nu)} \left(\frac{1}{L}\right)^{1/2} \begin{Bmatrix} \Delta_1 \\ \Delta_2 \end{Bmatrix}, \tag{22}$$

where

$$\Delta_1 = 4(u_{x6} - u_{x4}) - (u_{x3} - u_{x2}), \tag{23}$$

$$\Delta_2 = 4(u_{z6} - u_{z4}) - (u_{z3} - u_{z2}), \tag{24}$$

and ν is the Poisson's ratio of the material. In the above equations u_{xi} and u_{zi} represent the displacement components at the ith node. The nodes 2, 3, 4, and 6 along with L were defined in Liu et al. (1996).

With the solutions in frequency domain at hand, the time domain responses of the medium can be easily recovered by inverse Fourier transform.

6. Results and discussions

Two vertical cracks with length d are considered in this study. One is a surface-breaking crack and the other is a sub-surface crack which is $d/4$ deeper than the surface-breaking crack. All computations have been carried out for a value of Poisson's ratio $\nu = 1/3$. The variables used in this study are presented in nondimensional form. The spatial coordinates are normalized with respect to the crack length d. The wave velocities are normalized with respect to the shear wave velocity β. Thus the normalized shear wave velocity is equal to 1.0. Based on the value of Poisson's ratio, the corresponding normalized longitudinal and Rayleigh wave velocities can be estimated (Achenbach, 1973) to be 2.0 and 0.933, respectively. The normalized time ($\bar{t}$) and frequency ($\bar{f}$) are defined as

$$\bar{t} = \frac{t\beta}{d} \tag{25}$$

and

$$\bar{f} = \frac{fd}{\beta}, \tag{26}$$

where $f = \omega/2\pi$ is the frequency. The loading function is a Ricker pulse given by

$$p(t) = (2\pi^2 f_{\mathrm{c}}^2 t^2 - 1)\exp(-\pi^2 f_{\mathrm{c}}^2 t^2), \tag{27}$$

where f_{c} is the characteristic frequency of the pulse. Note that the load has its maximum value at $t = 0$. For all the numerical results presented in this paper, the loading function with normalized characteristic frequency equal to 1.0 is applied on the free surface at the point $x = -0.95d$, in which the wavelength of the shear wave is equal to the crack length d. To obtain the transient responses, the normalized frequency range of 0.0–4.0 was equally subdivided into 65 discrete frequencies and the response was then computed at each of these frequencies. The responses in frequency domain are given by multiplying these spectra by the

spectrum of the loading function. The corresponding responses in time domain is then obtained by using the fast Fourier transform. First, the numerical accuracy was checked by means of performing the zero-scattering test. Very good agreement has been obtained. Besides, for the anti-plane problem with a surface-breaking crack, very consistent results were shown in Liu et al. (1997) for the crack opening displacements and the stress intensity factors at different frequencies in comparison with those presented by Stone et al. (1980). The numerical results for the loading function applied in x- and z-directions are discussed separately in the next two sub-sections.

6.1. Force in the x-direction

The horizontal and vertical displacements from $x/d = -2.0$ to 2.0 on the surface of a medium without the crack are shown in Figs. 2 and 3, respectively. Note that the results shown in Figs. 2 and 3 are computed from analytical solutions. Those computed from the hybrid numerical method (not shown here) also have very good agreement with Figs. 2 and 3. This is so called zero-scattering test. In view of these figures, it is clear that the longitudinal (P), shear (SV), and Rayleigh (R) waves are generated from the impact source. According to the problem considered in this study, these initial waves will arrive at $x/d = -2.0$ and 2.0 at

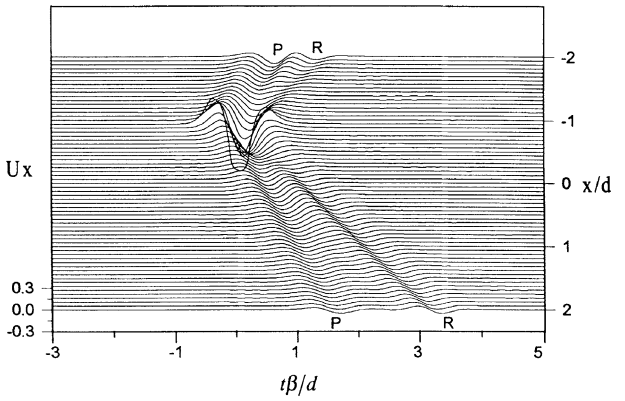

Fig. 2. Horizontal displacements at the free surface of a homogeneous medium subjected to a force in the x-direction.

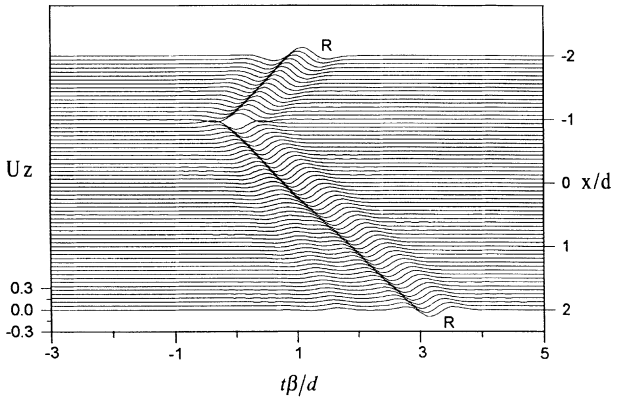

Fig. 3. Vertical displacements at the free surface of a homogeneous medium subjected to a force in the x-direction.

about $\bar{t} = 0.525, 1.05, 1.125$ and $\bar{t} = 1.475, 2.95, 3.162$, respectively. These results can be confirmed from the figures. The longitudinal and Rayleigh waves can be easily distinguished in Fig. 2 from their quite different wave velocities. However, the vertical surface displacements shown in Fig. 3 are mainly the coupling of Rayleigh waves and shear waves due to their similar wave velocities. It is observed that Rayleigh surface waves dominate the elastodynamic field near the free surface because most of the energy of the Rayleigh waves is confined to the free surface while the energy of body waves (longitudinal and shear waves) are spread over the entire domain. Therefore the Rayleigh waves are useful information for the detection of the near surface flaws because they can be easily accessible to measurement with a transducer on the surface.

The horizontal surface displacements of a medium containing a surface-breaking crack and a sub-surface crack are shown in Figs. 4 and 5, respectively. It is observed that the responses before the initial waves interact with the cracks are consistent with those of homogeneous medium as shown in Fig. 2. This can be considered as another way to verify the reliability of the hybrid numerical method. After the initial waves interact with the cracks, they are reflected and diffracted by the cracks. For the problem considered here, the blocking effect of the surface-breaking crack to the initial waves is much stronger than that of the sub-surface crack. Thus the patterns of the surface responses caused by a surface-breaking crack are quite

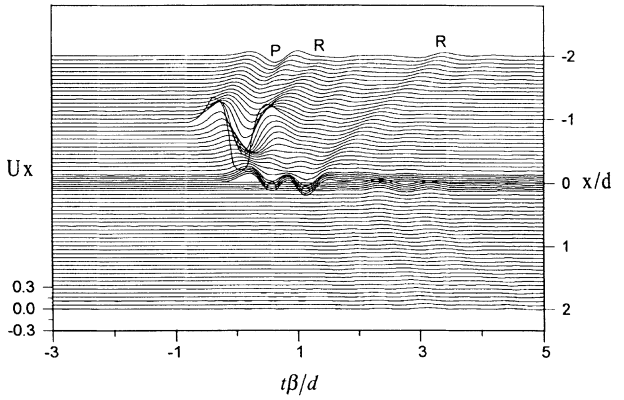

Fig. 4. Horizontal displacements at the free surface of a medium containing a vertical surface-breaking crack with force in the x-direction.

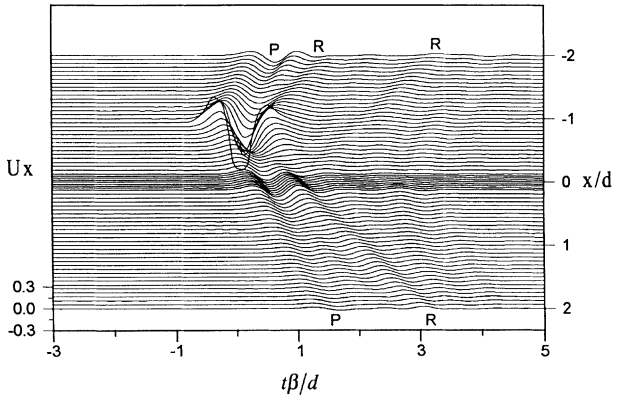

Fig. 5. Horizontal displacements at the free surface of a medium containing a vertical sub-surface crack with force in the x-direction.

distinct from those caused by a sub-surface crack. These differences are useful for the classification of the crack types. Although the diffracted waves from the lower crack-tips are weak compared with other waves, they can be clearly observed at the free surface. Their amplitudes and arrival times are strongly related to the locations of the crack-tips.

Figs. 6 and 7 show the horizontal crack opening displacements along the whole crack length of the surface-breaking and sub-surface cracks, respectively. The amplitudes of crack opening displacements for the surface-breaking crack are very large at the crack mouth when the initial waves arrive at the crack. After the initial waves, the effect of scattering waves can be observed from both figures. The crack opening displacements near the crack-tips, which vary rapidly when the initial waves arrive, are closely related to the stress intensity factors. The dynamic stress intensity factors (K_I and K_{II}) for the surface-breaking crack are shown in Fig. 8. It is shown that K_I has larger amplitude and oscillates longer than K_{II}. Figs. 9 and 10 show the dynamic stress intensity factors K_I and K_{II} for the sub-surface crack, respectively. The upper tip has larger values of K_I and K_{II} when the initial waves arrive at the crack. However, a very interesting result is found in Fig. 9. The lower tip could have larger value of K_I in the time histories than the upper tip. This phenomenon was not found in the case of the Rayleigh wave incidence alone as shown in Fig. 10(b) in Liu et al. (1996).

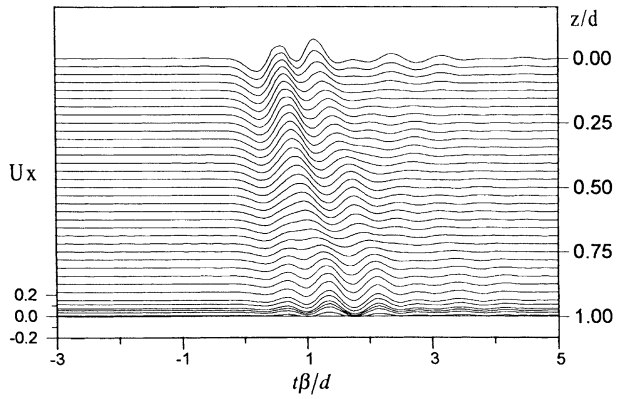

Fig. 6. Horizontal crack opening displacements for the vertical surface-breaking crack with force in the x-direction.

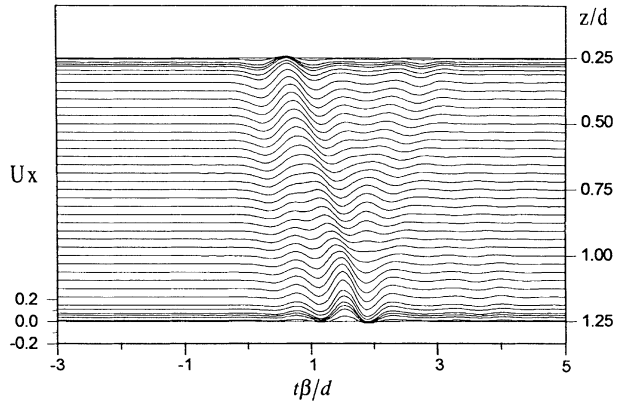

Fig. 7. Horizontal crack opening displacements for the vertical sub-surface crack with force in the x-direction.

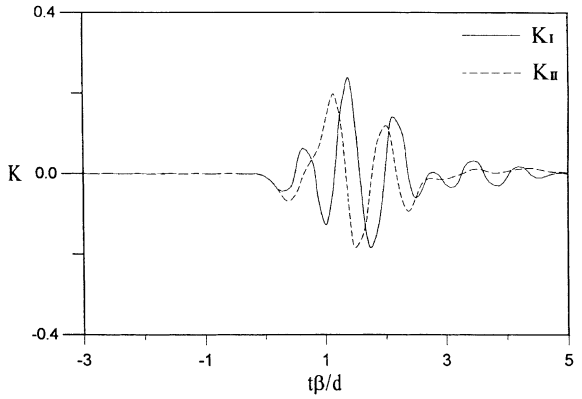

Fig. 8. Dynamic stress intensity factors for the vertical surface-breaking crack with force in the x-direction.

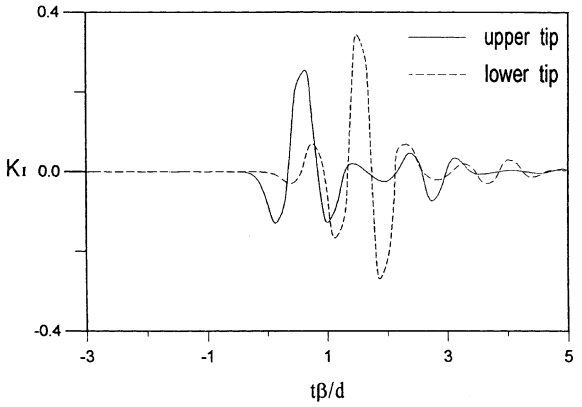

Fig. 9. Dynamic stress intensity factors (K_{I}) for the vertical sub-surface crack with force in the x-direction.

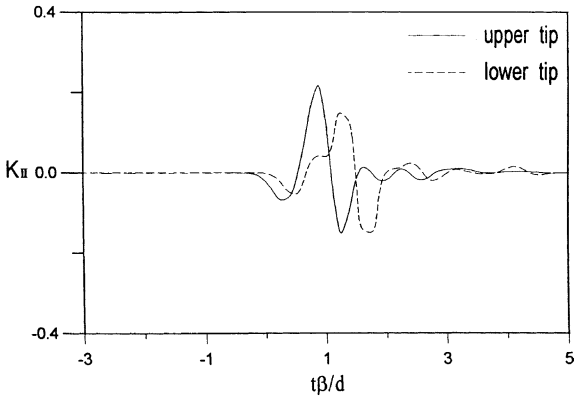

Fig. 10. Dynamic stress intensity factors (K_{II}) for the vertical sub-surface crack with force in the x-direction.

6.2. Force in the z-direction

Generally speaking, the patterns of the responses for the case of force in the z-direction are similar to those for the case of force in the x-direction. Figs. 11 and 12 computed from analytical solutions show the horizontal and vertical surface displacements on a medium without the crack, respectively. It is shown again that among the initial waves Rayleigh waves have more contribution to the surface responses than longitudinal and shear waves. Compared with Fig. 2, the longitudinal wave is not obvious in Fig. 11.

The vertical surface displacements of a medium containing a surface-breaking crack are shown in Fig. 13. The initial Rayleigh waves are reflected as Rayleigh waves. Later, the diffracted waves from the crack-tip appear at the free surface. Fig. 14 shows the vertical surface displacements for the case with a sub-surface crack. In this case, reflected waves, transmitted waves, and diffracted waves from both crack-tips are observed at the free surface. Diffracted waves induced by the upper crack-tip and transmitted waves are mixed together in the region $x > 0$. Note that the accuracy of the developed method used in this paper are ensured again by comparing the analytical results shown in Fig. 12 with the numerical results before the initial waves arrive at the cracks as shown in Figs. 13 and 14.

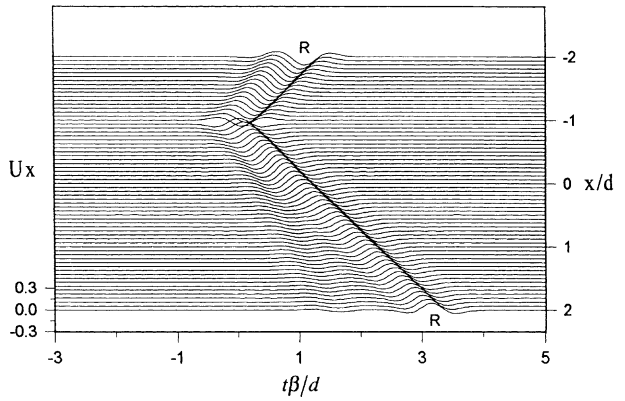

Fig. 11. Horizontal displacements at the free surface of a homogeneous medium subjected to a force in the z-direction.

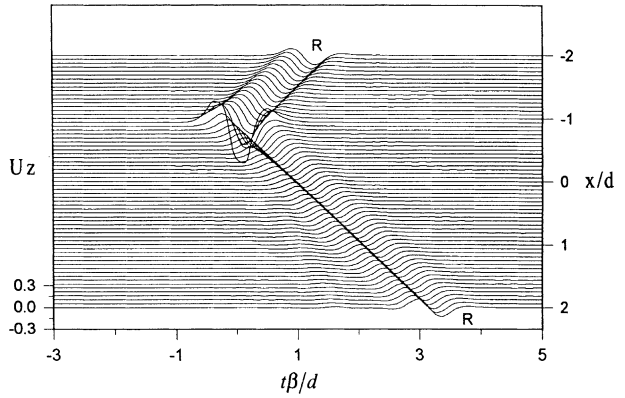

Fig. 12. Vertical displacements at the free surface of a homogeneous medium subjected to a force in the z-direction.

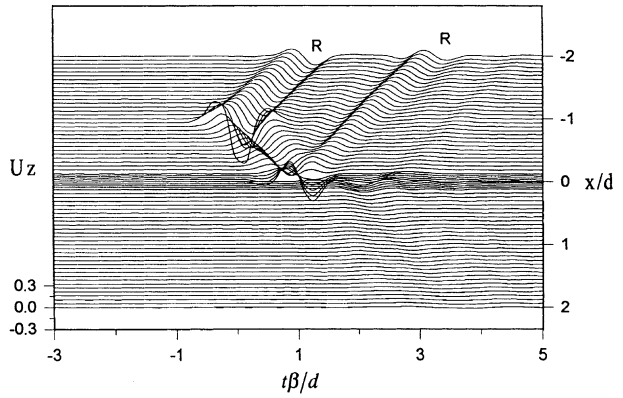

Fig. 13. Vertical displacements at the free surface of a medium containing a vertical surface-breaking crack with force in the z-direction.

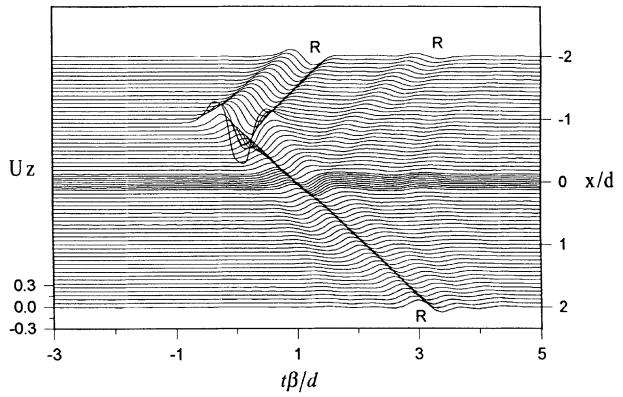

Fig. 14. Vertical displacements at the free surface of a medium containing a vertical sub-surface crack with force in the z-direction.

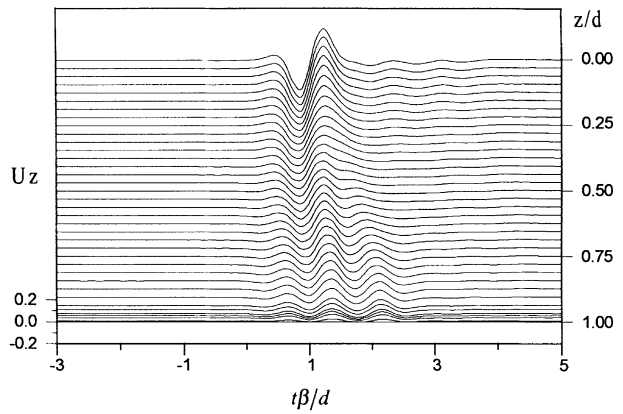

Fig. 15. Vertical crack opening displacements for the vertical surface-breaking crack with force in the z-direction.

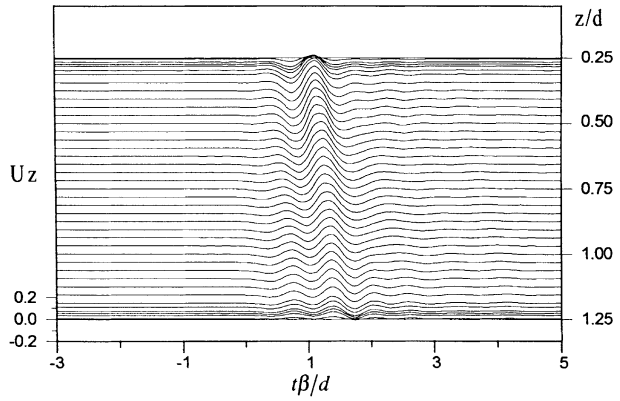

Fig. 16. Vertical crack opening displacements for the vertical sub-surface crack with force in the z-direction.

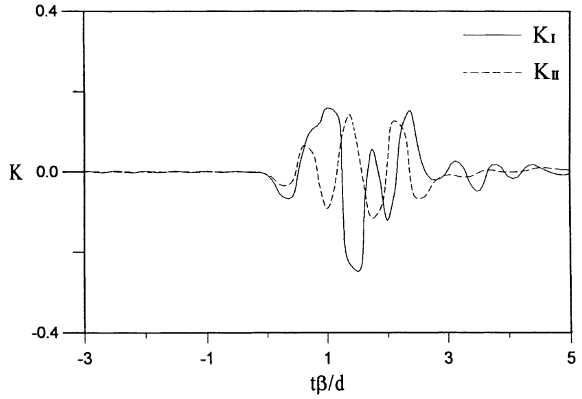

Fig. 17. Dynamic stress intensity factors for the vertical surface-breaking crack with force in the z-direction.

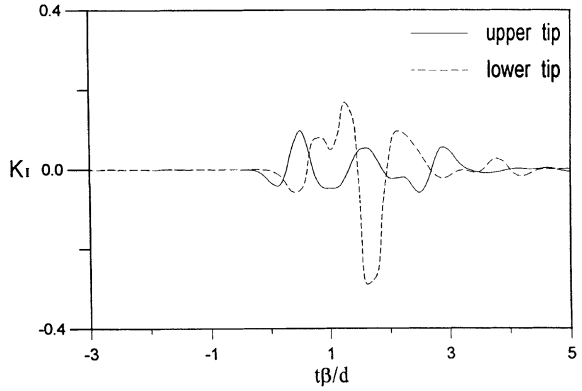

Fig. 18. Dynamic stress intensity factors (K_I) for the vertical sub-surface crack with force in the z-direction.

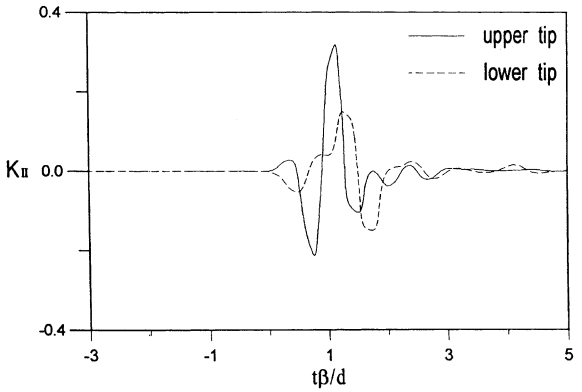

Fig. 19. Dynamic stress intensity factors (K_{II}) for the vertical sub-surface crack with force in the z-direction.

The vertical crack opening displacements for the surface-breaking and sub-surface cracks are shown in Figs. 15 and 16, respectively. Large crack opening displacements are observed at the crack mouth as shown in Fig. 15. Dynamic stress intensity factors for the surface-breaking crack are shown in Fig. 17 and those for the sub-surface crack are shown in Figs. 18 and 19. It is observed again in Fig. 18 that the stress intensity factor (K_I) at the lower tip of the sub-surface crack has much larger amplitude than the upper tip. This could be the contribution from the body waves.

7. Conclusions

A hybrid method combining the finite element method with boundary integral equation is applied to investigate the dynamic responses of a cracked elastic solid subjected to in-plane surface loadings. The numerical results for surface displacements, crack opening displacements, and dynamic stress intensity factors are presented. The initial waves generated by the loading pulse include longitudinal, shear, and Rayleigh waves. Among the initial waves Rayleigh surface waves dominate the elastodynamic field near the free surface because most of the energy of Rayleigh waves is restricted to the free surface while the energy of body waves are spread into the entire domain. The patterns of the surface responses caused by a surface-breaking crack are quite distinct from those caused by a sub-surface crack. The distinctions can be used to classify the types of cracks. The amplitudes and arrival times of the diffracted waves from the crack-tips are strongly related to the location and size of the crack. The lower tip of the sub-surface crack could have larger value of K_I in the time histories than the upper tip. This phenomenon does not occur in the case of the Rayleigh wave incidence alone. This contribution is mainly from the body waves.

Acknowledgements

The authors would like to thank the National Science Council of the Republic of China for financially supporting this research under contract Nos. NSC 89-2212-E-035-004, NSC 89-2212-E-035-015, and NSC 90-2811-E-035-001.

References

Achenbach, J.D., 2000. Quantitative nondestructive evaluation. Int. J. Solids Struct. 37, 13–27.
Achenbach, J.D., 1973. Wave Propagation in Elastic Solids. North-Holland, Amsterdam.
Boström, A., Jansson, P.-Å., Olsson, P., 1994. Antiplane elastic wave scattering from a curved randomly rough crack. J. Appl. Mech. 61, 835–842.
Datta, D., Kishore, N.N., 1996. Features of ultrasonic wave propagation to identify defects in composite materials modeled by finite element method. NDT E Int. 29 (4), 213–223.
Datta, S.K., 1979. Diffraction of SH-waves by an edge crack. J. Appl. Mech. 46, 101–106.
Georgiadis, H.G., Brock, L.M., 1994. Exact elestodynamic analysis of some fracture specimen models involving strip geometries. Int. J. Solids Struct. 31 (19), 2599–2613.
Harumi, K., Uchida, H., 1990. Computer simulation of ultrasonics and its applications. J. Nondestruct. Eval. 9 (2/3), 81–99.
Kishore, N.N., Sridhar, I., Iyengar, N.G.R., 2000. Finite element modeling of the scattering of ultrasonic waves by isolated flaws. NDT E Int. 33, 297–305.
Liu, S.W., Sung, J.C., Chang, C.S., 1996. Transient scattering of Rayleigh waves by surface-breaking and sub-surface cracks. Int. J. Engng. Sci. 34 (9), 1059–1075.
Liu, S.W., Sung, J.C., Chang, C.S., 1997. Transient scattering of SH waves by surface-breaking and sub-surface cracks. Int. J. Solids Struct. 34 (30), 4019–4035.
Liu, S.W., Sung, J.C., Chang, C.S., 1998. Responses of a cracked half-space subjected to an antiplane impact. Engng. Struct. 20 (9), 819–825.
Ma, C.C., Chen, S.K., 1994. Exact transient full-field analysis of an antiplane subsurface crack subjected to dynamic impact loadings. J. Appl. Mech. 61, 649–655.
Saenger, E.H., Gold, N., Shapiro, S.A., 2000. Modeling the propagation of elastic waves using a modified finite-difference grid. Wave Motion 31, 77–92.
Saffari, N., Bond, L.J., 1987. Body to Rayleigh wave mode-conversion at steps and slots. J. Nondestruct. Eval. 6 (1), 1–22.
Scandrett, C.L., Achenbach, J.D., 1987. Time-domain finite difference calculations for interaction of an ultrasonic wave with a surface-breaking crack. Wave Motion 9, 171–190.
Shah, A.H., Wong, K.C., Datta, S.K., 1986. Dynamic stress intensity factors for buried planar and nonplanar cracks. Int. J. Solids Struct. 22 (8), 845–857.
Stone, S.F., Ghosh, M.L., Mal, A.K., 1980. Diffraction of antiplane shear waves by an edge crack. J. Appl. Mech. 47, 359–362.
Tsai, C.H., Ma, C.C., 1993. The stress intensity factor of a subsurface inclined crack subjected to dynamic impact loading. Int. J. Solids Struct. 30 (16), 2163–2175.
Wang, L., Shen, J., 1997. Scattering of elastic waves by a crack in an isotropic plate. Ultrasonics 35, 451–457.
Xu, P.-C., Mal, A.K., 1987. Calculation of the inplane Green's functions for a layered viscoelastic solid. Bull. Seismic Soc. Am. 77, 1823–1837.
Zhang, Ch., 2000. Transient elastodynamic antiplane crack analysis of anisotropic solids. Int. J. Solids Struct. 37, 6107–6130.